The JVAS/CLASS search for 6-arcsec to 15-arcsec image separation lensing

Phillips, P. M.; Browne, I. W. A.; Jackson, N. J.; Wilkinson, P. N.; Mao, S.; Rusin, D.; Marlow, D. R.; Snellen, I.; Neeser, M.

Published in:
Monthly Notices of the Royal Astronomical Society

DOI:
10.1046/j.1365-8711.2001.04601.x

Publication date:
2001

Mon. Not. R. Astron. Soc. **328,** 1001–1015 (2001)

The JVAS/CLASS search for 6-arcsec to 15-arcsec image separation lensing

P. M. Phillips,[1] I. W. A. Browne,[1★] N. J. Jackson,[1] P. N. Wilkinson,[1] S. Mao,[1] D. Rusin,[2] D. R. Marlow,[2] I. Snellen[3] and M. Neeser[4]

[1]*University of Manchester, Jodrell Bank Observatory, Macclesfield, Cheshire SK11 9DL*
[2]*University of Pennsylvania, Department of Physics and Astronomy, 209 South 33d Street, Philadelphia PA 19104, USA*
[3]*Institute of Astronomy, Madingley Road, Cambridge CB3 0HA*
[4]*Kapteyn Astronomical Institute, Postbus 800, 9700 AV Groningen, the Netherlands*

Accepted 2001 April 17. Received 2001 April 10; in original form 2000 November 27

ABSTRACT

The Jodrell Bank–VLA Astrometric Survey (JVAS) and the Cosmic Lens All Sky Survey (CLASS) have been systematically searched for multiple gravitational imaging of sources with image separations between 6 arcsec and 15 arcsec, associated with galaxy group and cluster lensing masses. The radio and optical follow-up observations of all candidates are presented. From a total of ∼15 000 sources only one weak candidate remains and this is *not* contained in the statistically complete sample of flat-spectrum JVAS/CLASS sources of 11 670 sources. A simple Press–Schechter analysis is performed. For singular isothermal sphere lenses the lack of multiple image systems is inconsistent with the currently favoured cosmologies with $(\Omega_{\rm M}, \Omega_\Lambda) = (0.3, 0.7)$ at the 4.2σ level. Cored isothermal lenses reduce the expected number of lens systems and we suggest that the most probable interpretation of our results is that the surface mass density of groups and clusters of galaxies is not high enough to cause multiple imaging and the presence of the mass concentrations associated with individual galaxies is required to produce image separations such as those in B0957+561.

Key words: gravitational lensing – galaxies: clusters: general – dark matter.

1 INTRODUCTION

So far 18 lens systems have been confirmed in the Jodrell Bank – Very Large Array (VLA) Astrometric Survey (JVAS: Patnaik et al. 1992; Browne et al. 1998; Wilkinson et al. 1998) and Cosmic Lens All Sky Survey (CLASS; Myers et al. 1995). These resulted from the systematic follow up of candidates with image separations of 0.3 arcsec $\leq \Delta\theta \leq$ 6 arcsec, associated with galaxy-scale lensing masses.[1] The sources in the statistically complete JVAS/CLASS sample were selected to have $S_5 \geq 30$ mJy in the Greenbank 5-GHz catalogue (GB6; Condon, Broderick & Seielstad 1989) and spectral index $\alpha \geq -0.5$ (where $S \propto \nu^\alpha$) between the NRAO VLA Sky Survey 1.4-GHz catalogue (NVSS; Condon et al. 1998) and the GB6 catalogue. This results in a sample size of 11 685 sources, of which 11 670 have been observed with the VLA in A configuration at 8.4 GHz. It is possible to examine the fields around each JVAS/CLASS source to greater angular distances. With this in mind, the maximum search radius for lens candidates has been expanded from 6 to 15 arcsec; this corresponds to lensing by groups and small clusters of galaxies with masses of $\sim 10^{13}\,{\rm M}_\odot$ ($\sigma_v \sim 500\,{\rm km\,s^{-1}}$). An additional ∼3000 sources had been selected and observed with the VLA prior to the appearance of the NVSS catalogue and these are *not* part of the complete sample defined above. However, all ∼15 000 observed sources have been examined for lensing on the scale of 6 to 15 arcsec.

It would be possible to search to even greater radii with the JVAS/CLASS VLA data. However, one problem encountered when searching for such large separation lensing events is the significant increase in the level of contamination by random associations of sources presenting themselves as lens candidates. A second problem is the fact that the path lengths to two lensed images of a background source are different unless the lens and source are perfectly aligned; this results in a time delay between the two images. Flat-spectrum radio sources are typically very compact and as a result the radio source structure and flux density can change significantly over the time-scale of the time delay. For the case of image separations of 60 arcsec this time delay can be of the order of hundreds of years. Thus, the two images could appear to have significantly dissimilar properties, and one runs the risk of rejecting real lens systems on this basis. As a result of the considerations above a conservative upper image separation of 15 arcsec was imposed on the lens search reported here.

★E-mail: iwb@jb.man.ac.uk

[1] JVAS and CLASS lens survey papers can be found at URL http://gladia.astro.rug.nl:8000/ceres/papers/papers.html

Statistics on the prevalence of lensing events relate to the clumpiness of matter in the universe and provide constraints on the cosmological parameters. The analysis of the statistics of 0.3 arcsec $\leq \Delta\theta \leq$ 6 arcsec lensing events, associated with galaxy-scale masses, typically assumes that the lens population is essentially non-evolving. Searching for lensing by groups and clusters of galaxies provides a different perspective on these parameters, as the relevant mass scales *are* evolving at lens redshifts. Numerical simulations of dark matter haloes show that the number of >5 arcsec image separation lensing events detectable in a sample can change by orders of magnitude depending on the cosmological model being used (for example Cen et al. 1994). Using a cosmological model with $\Omega_{\rm M} = 1$, $\Omega_\Lambda = 0$ and $H_0 = 50\,{\rm km\,s^{-1}\,Mpc^{-1}}$, Wambsganss et al. (1995) predicted that image splittings larger than 5 arcsec should be common. Based on the calculations of Wambsganss et al. (1995) one might expect to observe ~5 systems with image separations 6 arcsec $\leq \Delta\theta \leq$ 15 arcsec within the JVAS and CLASS samples.

Section 2 gives an overview of the methodology used to find gravitational lens candidates from the 8.4-GHz JVAS/CLASS data set. Section 3 contains a description of the way in which candidates are eliminated through follow-up observations with the VLA and MERLIN, while in Section 4 there is a discussion of the general implications of the results of the search. The constraints that the lack of wide-separation lens systems place on the core radii of galaxy groups and clusters are analysed in Section 5.

2 INITIAL CANDIDATE SELECTION

The JVAS and CLASS sources have all been observed with the VLA in A configuration at 8.4 GHz. These observations were carried out and analysed in several phases between 1990 February and 1999 August. After the fourth and final phase of CLASS 8.4 GHz observations, the entire data set was re-flagged and recalibrated in a standard way within the National Radio Astronomy Observatory (NRAO) Astronomical Image Processing System (AIPS) software package, to ensure uniformity over all epochs of observations. The data were then mapped using an automatic script within DIFMAP (Shepherd 1997; Pearson et al. 1994) and Gaussian model components were fitted to the data. The typical rms noise achieved was 200 μJy beam^{-1}.

The methodology for 6- to 15-arcsec candidate selection was the same as that used for the selection of lens candidates from the JVAS/CLASS sample with image separations of 0.3 arcsec $\leq \Delta\theta \leq$ 6 arcsec. The Gaussian components fitted to the 8.4-GHz VLA data within DIFMAP were used as a quantitative measure in this process. Sources were selected which had multiple 'compact' components with flux ratios ≤10:1. The beamsize of the VLA at 8.4 GHz in A configuration is ~0.2 arcsec. A compact component was defined in which the FWHM of the major axis ≤170 mas; this is an arbitrary but conservative definition of compactness. Only those systems with a combined flux density in all components of ≥20 mJy at 8.4 GHz were selected for practical reasons in the follow-up. This reduces the complete sample to 9261 sources. The selection of candidates was implemented by an automatic candidate generator *and* by a visual inspection of all maps with multiple components, regardless of component sizes and flux densities. By this method it was possible to reject sources selected by the automatic candidate generator which contained obvious core–jet or similar structure, indicative of the components being part of the same source. In addition it was possible to identify and re-map by hand any sources with confusing side-lobe structures which may have been included by the automatic candidate generator. This exhaustive process resulted in the selection of 13 candidate lens systems with component separations in the range 6 arcsec $\leq \Delta\theta \leq$ 15 arcsec (see Table 1). In fact, only 10 sources strictly meet the selection criteria described above. J0958+298, J1000+278 and J1326+607 were followed up as borderline but interesting candidates.

Table 1. A summary of the thirteen 6 arcsec $\leq \Delta\theta \leq$ 15 arcsec lens candidates from the total JVAS/CLASS data set of ~15 000 sources. Columns 2 and 3 give the right ascension and declination of the brightest 8.4-GHz component in J2000 coordinates. Column 4 shows the component separation in arcsec, column 5 shows the total 8.4-GHz flux density in mJy, while column 6 shows the flux density ratio between the two components. Note that the total flux density quoted is for the two compact components only. Also note that J0958+298, J1000+278 and J1326+607 do not strictly meet the selection criteria given in the text.

Name	RA (J2000)	Dec. (J2000)	$\Delta\theta$	$S_{\rm total}$	S_A/S_B
J0051+122	00 51 36.761	+12 12 53.168	11.5	32.6	3.1
J0122+427	01 22 24.735	+42 45 21.109	9.9	21.3	1.4
J0255+026	02 55 31.014	+02 40 30.440	12.3	21.4	1.4
J0958+298	09 58 58.950	+29 48 04.180	8.5	92.8	14.7
J1000+278	10 00 29.146	+27 52 12.172	9.9	69.6	11.1
J1212+739	12 12 40.779	+73 56 40.375	9.7	21.6	1.3
J1240+262	12 40 02.142	+26 17 20.680	12.8	24.8	2.2
J1326+607	13 26 43.913	+60 42 21.609	15.1	43.0	7.3
J1613+571	16 13 48.925	+57 11 02.469	7.4	24.3	1.1
J1940+519	19 40 56.917	+51 56 16.141	9.7	22.4	5.3
J2049+073	20 49 53.842	+07 18 59.441	7.2	21.9	4.2
J2255+434	22 55 11.258	+43 28 22.359	13.5	97.7	8.7
J2321+454	23 21 09.025	+45 25 42.438	13.6	23.1	4.6

Table 2. Stellar optical counterparts for the lens candidates detected on the APM. Note that both J0958+298 and J1000+278 have stellar optical counterparts for both components A and B. The separation from the 8.4-GHz radio component Δx is in milliarcsec, while both *R* (red) and *B* (blue) magnitudes are quoted where a detection is present.

Source	Component	Δx	m_R	m_B
J0051+122	A	–	–	–
	B	589	18.26	18.87
J0255+026	A	–	–	–
	B	147	18.95	20.50
J0958+298	A	117	19.47	19.19
	B	968	–	20.71
J1000+278	A	63	17.92	18.27
	B	300	–	20.60
J1240+262	A	523	–	21.13
	B	–	–	–
J1613+571	A	–	–	–
	B	342	17.12	17.74
J2049+073	A	708	18.21	18.73
	B	–	–	–

The Automatic Plate Measuring (APM) catalogue, derived from the POSS plates (for example, Irwin, Maddox & McMahon 1994), was searched around the components of the 13 lens candidates where survey coverage allowed. Two sources, J0958+298 and J1000+278, showed stellar optical counterparts at *both* radio component positions (see Table 2). The brightest radio component corresponds to the brightest optical counterpart in each system. However the flux density ratio of components in J0958+298 differs between radio and optical frequencies. The blue flux density ratio is 4.0 ± 1.0 whereas the 8.4-GHz flux density ratio is

Table 3. A summary of the Gaussian component parameters and rms noise levels in the maps of the sources followed up with the VLA at 1.4 and 15 GHz. Also listed are the Gaussian component parameters from the original 8.4-GHz JVAS/CLASS observations. The flux density S is quoted in mJy, the rms noise σ is in μJy beam^{-1}, while a is the fitted major axis of the Gaussian component in mas. Where extended emission has been fitted with more than one component we list the flux density and major axis of the component closest to the component in the 8.4-GHz map. For J0122+427 and J2321+454, the value of $\sigma_{1.4}$ is significantly lower than average, as it is with J0255+026 for $\sigma_{8.4}$ and σ_{15}. This is because additional observation time was obtained on these sources at the end of the allotted observing run.

Name	Comp.	$S_{1.4}$	$\sigma_{1.4}$	$a_{1.4}$	$S_{8.4}$	$\sigma_{8.4}$	$a_{8.4}$	S_{15}	σ_{15}	a_{15}
J0051+122	A	111.0	234	374	24.7	308	161	16.2	253	225
	B	14.9	234	785	7.9	308	76	6.6	253	95
J0122+427	A	8.3	85	427	12.6	272	97	12.9	251	33
	B	6.0	85	372	8.7	272	43	5.3	251	100
J0255+026	A	46.0	284	343	12.6	100	171	8.4	89	176
	B	9.3	284	553	8.8	100	42	9.6	89	51
J0958+298	A	88.8	363	285	86.9	199	32	89.3	280	31
	B	3.5	363	452	5.9	199	44	3.6	280	100
J1212+739	A	85.7	226	285	12.3	257	135	8.7	247	161
	B	66.7	226	278	9.4	257	148	7.1	247	134
J1240+262	A	28.7	253	428	17.0	178	44	20.1	298	95
	B	45.4	253	237	7.8	178	78	5.2	298	213
J1326+607	A	27.6	385	390	37.8	263	51	17.4	238	36
	B	29.7	385	466	5.2	263	163	3.2	238	174
J1613+571	A	58.0	549	307	12.8	312	152	7.7	242	149
	B	12.1	549	324	11.5	312	79	10.3	242	55
J1940+519	A	139.7	511	352	18.8	301	143	13.3	238	200
	B	16.5	511	705	3.6	301	121	3.0	238	246
J2255+434	A	70.5	205	112	87.6	283	23	60.0	255	21
	B	38.2	205	237	10.1	283	181	6.2	255	214
J2321+454	A	18.9	93	309	19.0	185	20	14.8	230	44
	B	1.0	93	1735	4.1	185	63	6.1	230	87

14.7 ± 1.5. Gravitational lensing is an achromatic phenomenon. There are, however, mechanisms such as extinction, scattering and intrinsic source variability that can affect the apparent brightness of lensed images, in particular at optical wavelengths. Thus these two systems were considered the strongest lens candidates at this stage. Consequently, MERLIN imaging and optical spectroscopy data were obtained of the strongest candidate, J1000+278, before the main follow-up phase of this project. These observations are described in Sections 3.2 and 3.4.

2.1 Selection effects

The sources in the JVAS and CLASS surveys have been selected based on their two-point spectral indices between 1.4 and 5 GHz. If there are any wide-separation lensing events within these surveys, the lensed sources will be behind an area of sky occupied by a group or cluster of galaxies acting as the lens. It is possible that there might be radio emission associated with the lensing mass itself, which would change the apparent spectral index of the background source, potentially causing it to be rejected from the initial survey. Radio emission from groups and clusters of galaxies could have two origins: diffuse radio emission from haloes or 'relics' of radio galaxies or discrete radio sources physically associated with objects within the group or cluster.

Diffuse cluster radio sources appear to be rare phenomena (Feretti & Giovannini 1996). For example, a recent survey of the 205 X-ray brightest Abell-type clusters using NVSS has found only 29 candidate diffuse cluster radio sources (Giovannini, Tordi & Feretti 1999). Typically these sources have flux densities $10\,\mathrm{mJy} < S_{1.4} < 100\,\mathrm{mJy}$ and angular sizes $2\,\mathrm{arcmin} < \theta < 8\,\mathrm{arcmin}$. As the lenses we expect are likely to be less rich clusters and at higher redshift than the clusters studied by Giovannini et al, any influence of such sources on the selection of JVAS and CLASS sources must therefore be small.

Zhao, Burns & Owen (1989) conducted a survey of nearby Abell clusters with the VLA at 1.4 GHz with the aim of detecting discrete radio cluster members and studying the properties of such sources in relation to the parent clusters. In ∼40 per cent of lower Abell richness class clusters (with < 50 cluster members, equivalent to the lensing masses investigated here), radio emission was detected at total radio powers $P_{1.4} > 3 \times 10^{23}\,\mathrm{W\,Hz^{-1}}$, corresponding to $S_{1.4} > 30\,\mathrm{mJy}$ at $z \sim 0.1$. At the most efficient lens redshifts of $0.1 < z < 0.5$ this detection rate would be significantly reduced. Furthermore, Cooray et al. (1998) examined 56 galaxy clusters and found an increase in the number density of radio sources at 28.5 GHz of ∼4 times the rate expected based on a 1.4-GHz survey of areas *without* rich clusters down to a 1.5-mJy flux density limit (Condon, Dickey & Salpeter 1990), or $\sim 78\,\mathrm{source\,deg^{-2}}$. This translates into a probability of just ∼2 per cent for such a source falling within an NVSS beam within such a cluster. As a result, the effect of discrete cluster radio sources acting against the selection of JVAS and CLASS background sources is assumed to be minimal.

3 FOLLOW-UP OBSERVATIONS

3.1 VLA observations

Eleven $6\,\mathrm{arcsec} \leq \Delta\theta \leq 15\,\mathrm{arcsec}$ lens candidates were observed with the VLA in A configuration during July and August 1999. The initial VLA 8.4 GHz observations of one candidate, J2049+073, did not take place until CLASS phase 4 on 1999 August 17, and so could not be selected until after this first phase of follow-up,

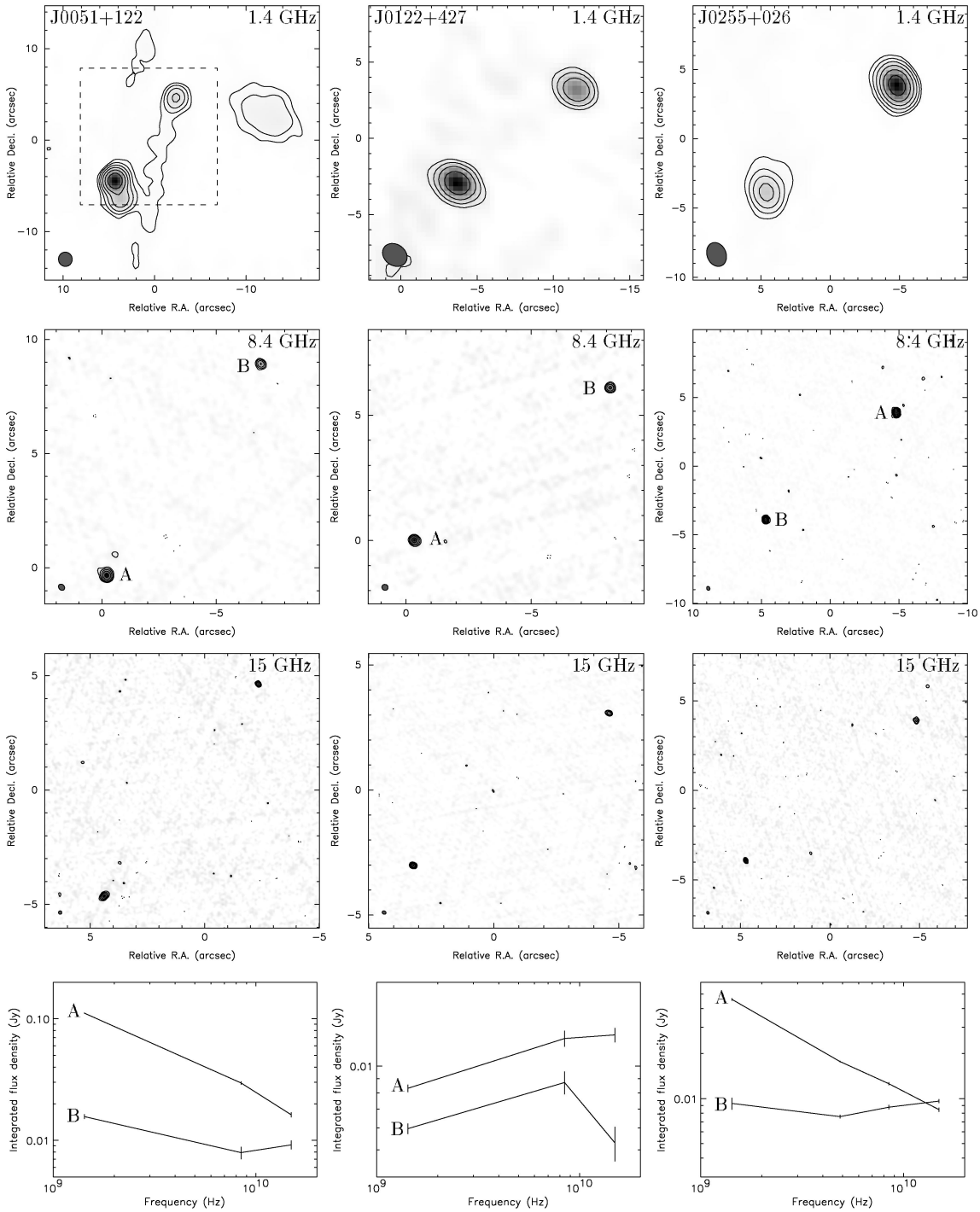

Figure 1. Maps of lens candidates observed during the VLA follow-up at 1.4 (top row) and 15 GHz (second row from bottom). Also shown are the original 8.4-GHz JVAS/CLASS maps (second row from top), and radio spectral plots (bottom row) based on the fitted Gaussian model parameters in each map. The contours are logarithmic with base 2 starting at 3σ, with the -3σ contour also plotted (see Table 3). The error bars in the radio spectra indicate the 3σ level in the map, and are not actual determinations of the error in the total flux density of a component. Sources shown are (left to right) (a) J0051+122, J0122+427, J0255+026; (b) J0958+298, J1212+739, J1240+262; (c) J1326+607, J1613+571, J1940+519 (the dashed box in the 1.4-GHz region shows the areas covered by the corresponding 8.4- and 15-GHz maps; (d) J2255+434, J2321+454.

however this candidate was followed up at the MERLIN stage of observations (see Section 3.2).

One candidate, J2049+073, was first observed during CLASS phase 4 on 1999 August 17 and so was not selected at this time. In addition, J1000+278 had been rejected as a lens candidate on the basis of optical spectroscopy (see Section 3.4). Observations were made at 1.4 GHz in an attempt to reveal any low-surface-brightness extended emission and to allow the identification of intrinsic double sources ('classical doubles') and at 15 GHz to provide higher resolution. The combined flux density information from the 1.4-GHz and 15-GHz observations, along with the original 8.4-GHz JVAS/CLASS data,

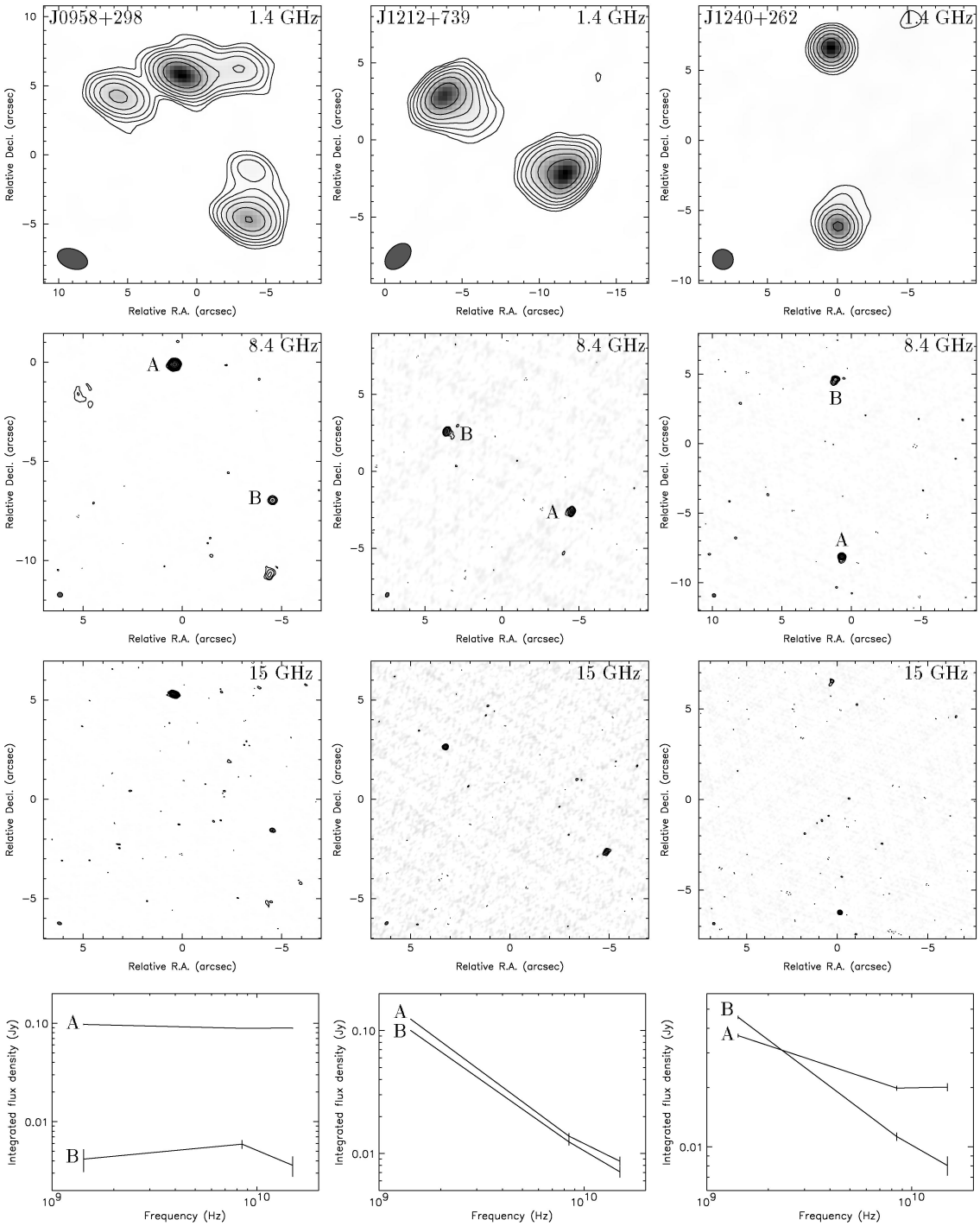

Figure 1 – *continued*

allowed comparisons to be made of the radio spectra of the putative lensed images.

Observations of 3C 286 and 3C 119 were made to calibrate the flux density scale. Flux densities of 14.75 and 8.60 Jy for 3C 286 and 3C 119 respectively were used at 1.4 GHz, while flux densities of 3.43 and 1.60 Jy were used at 15 GHz. Individual targets were observed for ∼1.5 min at 1.4 GHz and ∼5.5 min at 15 GHz. Standard VLA phase calibrators were observed before and after each target for ∼1.5 min. The data were edited and calibrated within AIPS in the standard way. The sources were mapped within DIFMAP and Gaussian model components were fitted to the visibility data to obtain quantitative parameters with which to assess the lens hypothesis in each case. Typical beam sizes were ∼150 mas and ∼1.5 arcsec at 15 and 1.4 GHz respectively. A summary of the putative lensed image parameters is given in Table 3, while the 1.4-GHz, 15-GHz and original CLASS 8.4-GHz maps are shown in Fig. 1.

Candidates are rejected as lens systems if the surface brightness of the two components is significantly different, if component spectral indices show gross differences or if components show

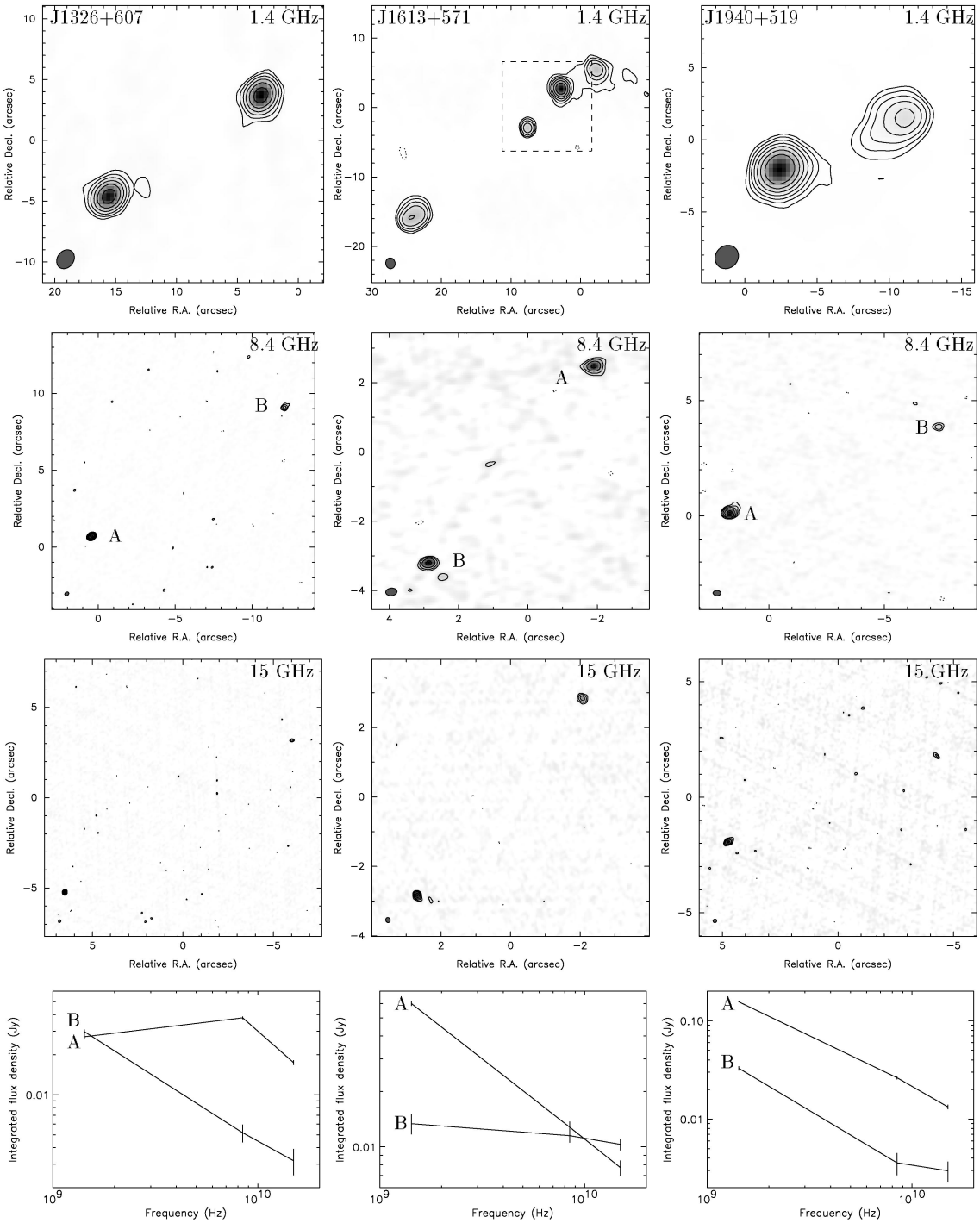

Figure 1 – *continued*

large differences in polarization. Further follow-up observations of candidates remaining after this stage are described in Sections 3.2 and 3.4. The status of each source observed in the VLA and/or MERLIN follow-up stages is summarized in Section 3.3.

3.2 MERLIN observations

The source J1000+278 was the strongest lens candidate from the JVAS/CLASS sample before any follow-up observations had been made, based on data from the APM catalogue (see Section 2). MERLIN observations were obtained at 5 GHz on 1999 February 7. The flux density scale was determined by a 30-min observation of 3C 286, and OQ 208 was observed for 40 min for use as a point-source calibrator, the flux of which was fixed by 3C 286. A flux density of 7.087 Jy was used for 3C 286, and thus a flux density of 2.31 Jy was derived for OQ 208. Phase calibration was achieved by 1.5-min observations every 5 min of a source selected from the JVAS list of bright point sources. The total time on source was 13.5 h, giving a theoretical rms noise of $\sim$47 μJy beam^{-1} and a beam size of 50×62 mas^2.

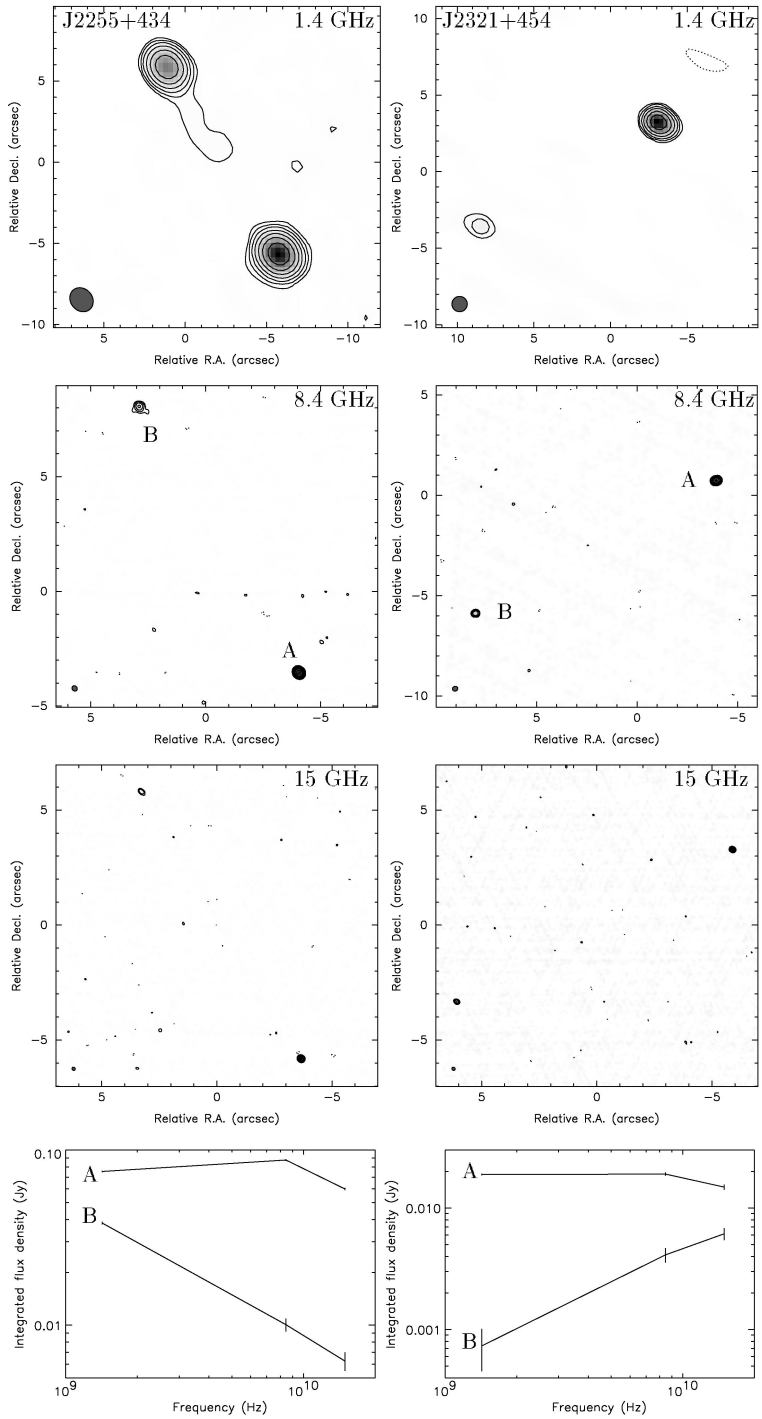

Figure 1 – *continued*

The three lens candidates remaining after the VLA follow-up (J0122+427, J0958+298 and J2049+073) were observed with MERLIN at 1.6 GHz between 1999 November 14 and 21. The flux density scale was determined by ∼30 min observations of 3C 286, and by ∼30 min observations of 2134+004, which was used as a point source calibrator. A flux density of 13.639 Jy was used for 3C 286, and thus a flux density of ∼5.08 Jy was derived for 2134+004. Phase calibrators were selected from JVAS. The total time on each source was 8.2, 10.6, and 7.2 h for J0122+427, J0958+298, and J2049+073 respectively. This gives a theoretical rms noise in each case of ∼73, 64 and 77 μJy beam^{-1}, with beam sizes of ∼160 mas.

The data were edited and calibrated using the standard MERLIN programs and AIPS. The data were then mapped within DIFMAP. Figs 2–5 show the total intensity maps of J0122+427, J0958+298, J1000+278, and J2049+073 respectively.

The status of each source observed with the VLA and/or MERLIN is summarized in the following section.

3.3 Individual source descriptions

J0051+122 (Fig. 1). The source shows extended structure at 1.4 GHz, including bridge emission between the putative lensed

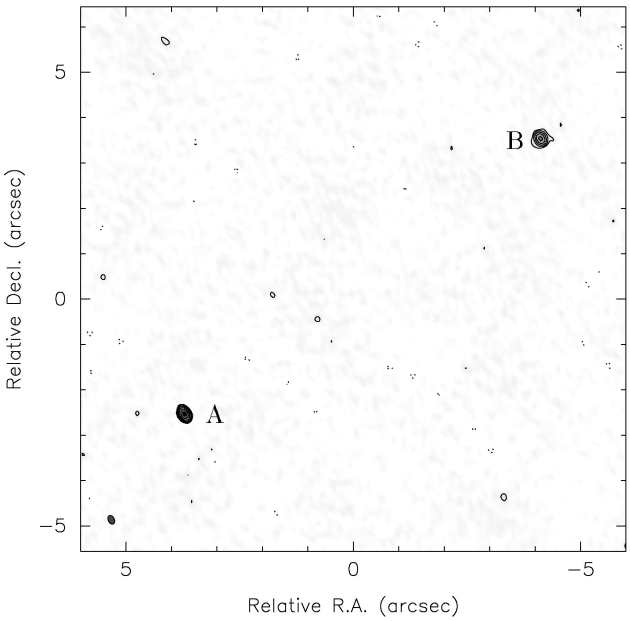

Figure 2. MERLIN 1.6-GHz map of J0122+427. Contours are logarithmic with base 2 starting at 3σ, plus -3σ. The beam size is 202×131 mas^2, while $\sigma = 101$ μJy beam^{-1}.

images, while at 8.4 and 15 GHz the components are unresolved. The radio spectra illustrate the fact that component A is probably a hotspot in a steep-spectrum lobe while B is the flat-spectrum core component. The source is rejected as a lens candidate.

J0122+427 (Fig. 1). The source shows two unresolved components at all frequencies [for example 97 mas (A) and 43 mas (B) at 8.4 GHz]. In addition, the radio spectra of the components are similar at lower frequencies. The difference in the flux density ratio at 15 GHz can plausibly be attributed to variability because this higher frequency emission is expected to originate from more compact structures. The lack of any resolved structure within either component means that this source remains a lens candidate.

(Fig. 2). Components A and B remain unresolved with MERLIN at 1.6 GHz with Gaussian component sizes of 42 and 79 mas respectively (c.f. the beam size of ∼160 mas). The source therefore remains a lens candidate.

J0255+026 (Fig. 1). The source has extended structure around the weaker component B at 1.4 GHz. In addition, the radio spectra are consistently different across the observed frequency range. The source is most likely a flat-spectrum core (B) with an unresolved bright steep-spectrum hotspot (A). The source is rejected as a lens candidate based on the lack of extended emission around component A at 1.4 GHz and the different radio spectrum of each component.

J0958+298 (Fig. 1). The source shows extensive extended structure at 1.4 GHz. Further resolved emission, coincident with emission at 1.4 GHz, is detected at 8.4 GHz, and marginally at 15 GHz to the south of component B. However, the putative lensed components have very similar flat-spectra across the observed frequency range and are unresolved [for example 32 mas (A) and 44 mas (B) at 8.4 GHz]. The resolution of the VLA 1.4-GHz map is not high enough confidently to reject the source as a lens candidate based on its morphology and so the source is retained as a lens candidate for the sake of caution.

(Fig. 3). Both components A and B have extended emission associated with them (boxed regions in figure) while B is unresolved (at 98 mas) and A contains possible 'jet' emission to the east of the peak in the MERLIN 1.6-GHz map. The surface brightnesses and morphologies of the extended emission associated with each component are inconsistent with them being lensed images of one another. In addition, the extended component associated with B is 20 per cent polarized, whilst there is no detected polarization on any other extended region. The source is therefore rejected as a lens candidate. Recently Lehar et al. (2001) published additional extensive radio and optical observations of J0958+298. Redshifts of $z = 2.064$ and $z = 2.744$ were derived for components A and B respectively. This confirms that J0958+298 can be conclusively rejected as a lens system.

J1000+278 (Fig. 4). Both components are unresolved with MERLIN at 5 GHz, with sizes of 14 and 12 mas. On the basis of the MERLIN data the source remains as a lens candidate, but optical spectra (also shown in Fig. 4 and discussed below) rule it out.

J1212+739 (Fig. 1). The source shows two resolved 'outer-edge-brightened' components at 1.4 GHz suggestive of two lobes of a single source. The steep-spectrum nature of these components adds further weight to this interpretation, despite the fact that they contain unresolved regions at 8.4 GHz [135 mas (A) and 148 mas (B)] and 15 GHz; these regions are likely to be hotspots in the lobes. The diffuse 1.4-GHz emission extending towards the centre of the system is not a plausible lensing morphology, and so the source is rejected as a lens candidate.

J1240+262 (Fig. 1). The source shows extended emission around component A at 1.4 GHz, which has a lower flux density than that of component B. However, B is resolved (213 mas) at 15 GHz while A is not. The radio spectrum of A is significantly flatter than that of B, suggesting that component A contains a flat-spectrum core of a single source with B being an associated steep-spectrum compact lobe. The source is rejected as a lens candidate.

J1326+607 (Fig. 1). The source has no extensive extended structure at any frequency. However, the radio spectra of the two components are significantly different with component A having a relatively flat spectrum, while the steep spectrum of component B gives the component flux ratio a range of ∼1 to ∼10 between 1.4 GHz and 15 GHz. The fact that B is also resolved (174 mas) at 15 GHz means that this source can be rejected as a lens candidate.

J1613+571 (Fig. 1). The source shows additional extended components in either direction to components A and B at 1.4 GHz. The radio spectra provide a strong argument against the lens hypothesis, as A has a steep spectrum compared with the relatively flat spectrum of B. Combined with the fact that A is marginally resolved (149 mas) at 15 GHz it is likely that the source is an FR II source, component B being the core. The source is thus rejected as a lens candidate.

J1940+519 (Fig. 1) The source shows extended structure around the weaker component B at 1.4 GHz. While the radio spectra of the two components are similar, surface brightness arguments can be applied at 1.4 GHz to reject the source as a lens candidate.

J2049+073 (Fig. 5). Component A at 158 mas is resolved with MERLIN at 1.6 GHz, while the weaker component B (at 94 mas) is 16 per cent polarized. Surface brightness arguments cannot be invoked in this case, however component A has no detectable polarization despite being more than twice as strong as B, and therefore the source is rejected as a lens candidate.

J2255+434 (Fig. 1). The source contains faint extended structure associated with component B at 1.4 GHz, in the direction towards component A. While this emission is only detected at the 3σ level, the radio spectra show B to be relatively steep-spectrum

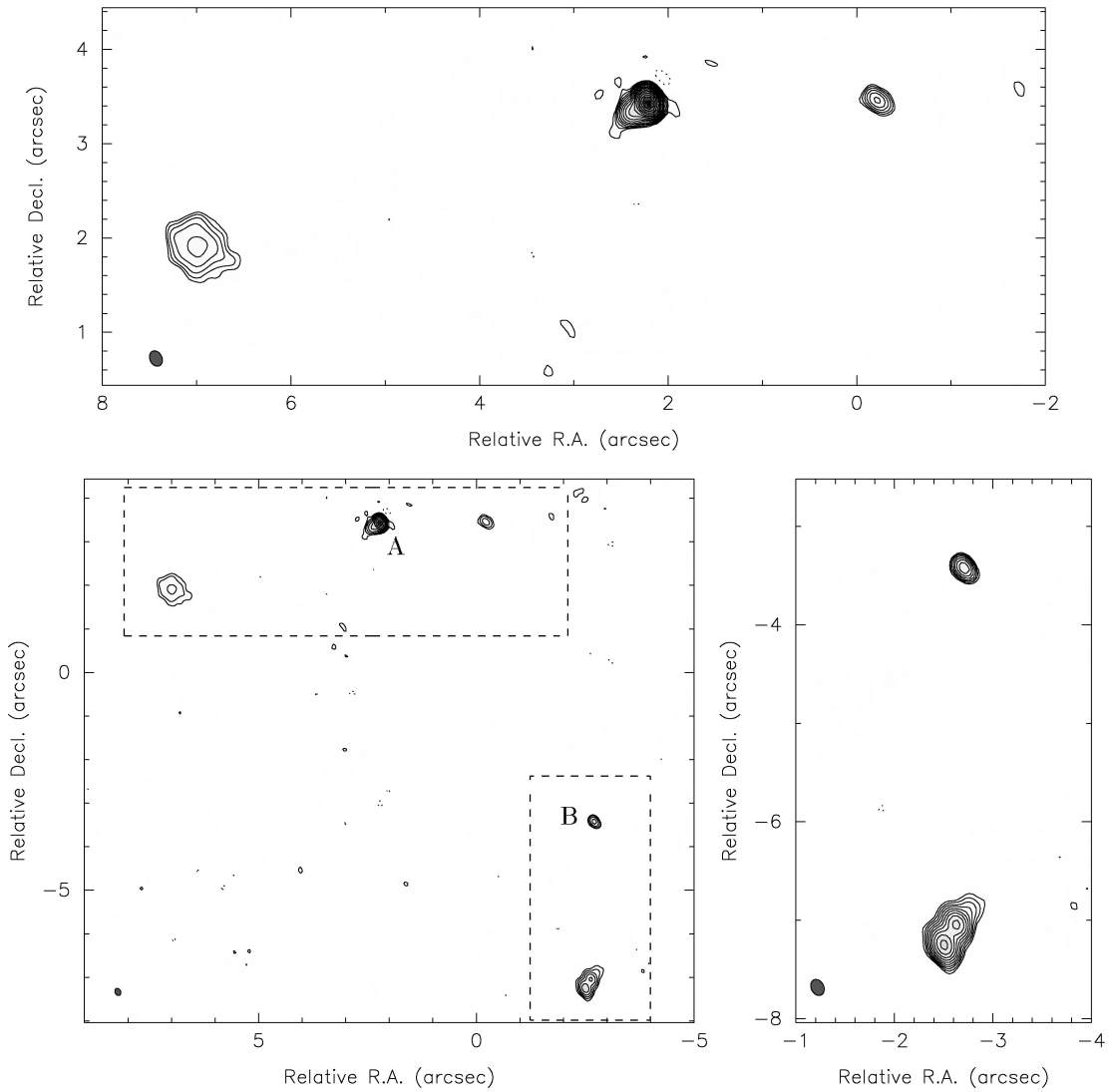

Figure 3. MERLIN 1.6-GHz maps of J0958+298. The bottom-left map shows the whole system while the top and bottom-right maps are enlargements of the two regions believed to be separate sources. Contours are logarithmic with base 2 for the bottom left map, while they are logarithmic with base $\sqrt{2}$ for the top and bottom-right maps. Contours start at 3σ, plus -3σ. The beam size is $128 \times 170\,\mathrm{mas}^2$, while $\sigma = 114\mu\mathrm{Jy\,beam}^{-1}$.

compared with the near flat-spectrum of A. Furthermore, B is slightly resolved (214 mas) at 15 GHz. Component A is most likely a flat-spectrum core with an associated steep-spectrum jet or lobe in B. The source is rejected as a lens candidate based on the differences in the radio spectra and the extended emission associated with component B.

J2321+454 (Fig. 1). The source shows no resolved structure at 8.4 and 15 GHz. However, the radio spectra show that component A has an almost flat spectrum, whilst the spectrum of component B is steadily increasing. Furthermore, B is slightly resolved (1.7 arcsec) at 1.4 GHz and so the source is rejected as a lens candidate.

3.4 Optical observations

Following the MERLIN observation of J1000+278, the source was observed spectroscopically with the William Herschel Telescope (WHT). The observations took place on 1999 February 23 using the red arm of the Intermediate dispersion Spectrograph and Imaging System (ISIS). The R300B grism providing $0.86\,\text{Å pixel}^{-1}$ was used giving a wavelength range of $\sim$3500 Å at a central wavelength of $\lambda_c = 4712$ Å. The total exposure time was 1500 s with the slit positioned over both components of the system.

The data reduction was carried out using the National Optical Astronomy Observatory (NOAO) Image Reduction and Analysis Facility (IRAF) software package in the standard way. Sky subtraction was performed prior to the extraction of each spectrum. A Cu–Ne arc spectrum was used for wavelength calibration, whilst flux calibration was performed using an observation of the spectrophotometric standard star Feige-34.

Each component of J1000+278 was found to contain two strong emission lines within the wavelength coverage of the instrumental set-up. Table 4 summarizes the results of Gaussian line fitting with the Starlink software package DIPSO. The unweighted mean redshift $\langle z \rangle$ was calculated from the redshift obtained from each fitted line. The final error on each redshift was estimated by combining the errors on the central wavelength from the Gaussian line-fitting procedure. Systematic errors in wavelength from the wavelength calibration have not been included. It can be clearly

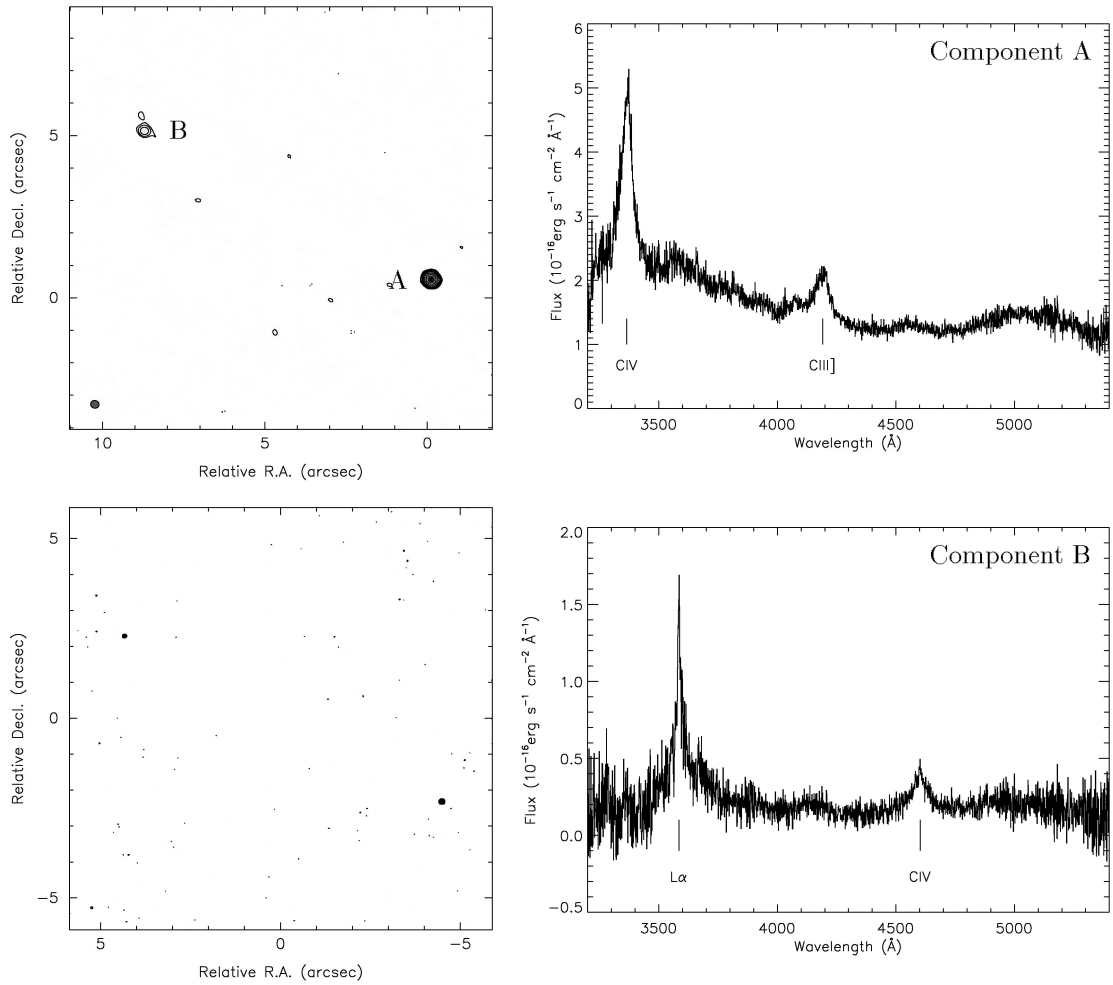

Figure 4. VLA 8.4-GHz (top left) and MERLIN 5-GHz (bottom left) maps of J1000+278. Contours are logarithmic with base 2 starting at 3σ, plus -3σ. The rms noise levels are $\sigma_{8.4} = 235\,\mu$Jy beam^{-1} and $\sigma_5 = 81\,\mu$Jy beam^{-1}. Also shown are the WHT optical spectra of component A (top right) and B (bottom right) of J1000+278.

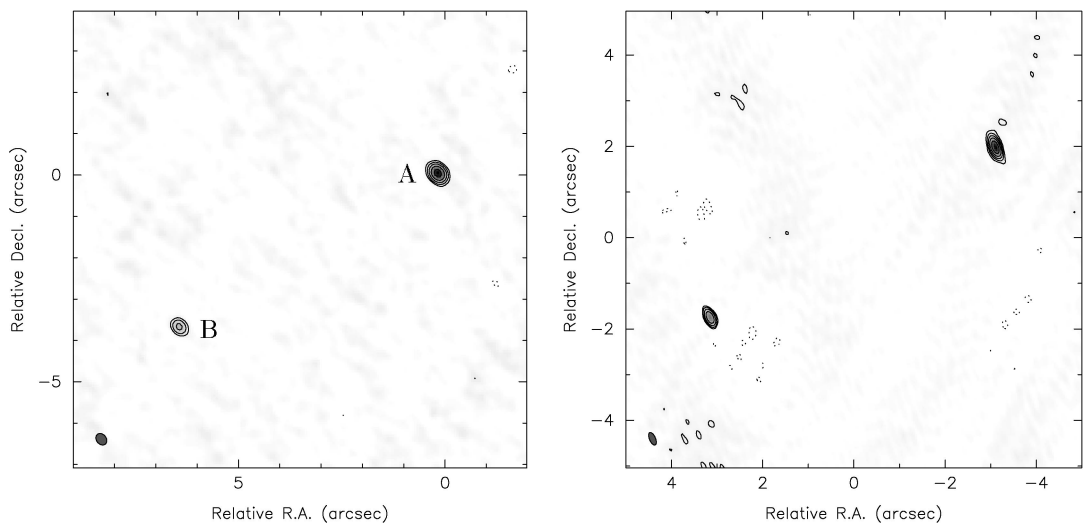

Figure 5. VLA 8.4-GHz (left) and MERLIN 1.6-GHz (right) maps of J2049+073. Contours are logarithmic with base 2 starting at 3σ, plus -3σ. The MERLIN beam size is 132×293 mas^2, while the rms noise levels are $\sigma_{8.4} = 264\,\mu$Jy beam^{-1} and $\sigma_{1.6} = 158\,\mu$Jy beam^{-1}. Note that component B has 16 per cent polarized emission at 1.6 GHz, whilst A has no detectable polarized emission.

Table 4. A summary of the spectroscopic results for J1000+278 obtained with the WHT. Shown for each component are the mean redshift from a combination of each emission line, each identified line, the observed and rest-frame wavelength of each line, and the fitted width (FWHM) of each line.

Comp.	$\langle z \rangle$	Line ID	$\lambda_{\rm obs}$ (λ_0) (Å)	FWHM (Å)
A	1.1839 ± 0.0003	CIV	3364.8 (1549)	56.2
		CIII]	4191.5 (1909)	76.3
B	1.9597 ± 0.0002	Lyα	3586.0 (1216)	26.7
		CIV	4601.0 (1549)	60.7

seen that the two components lie at two separate redshifts and are not physically related. J1000+278 can thus be rejected as a gravitational lens candidate. This illustrates the fact that the presence of two unresolved objects with similar radio spectra, and relatively similar radio to optical spectra, is not a sure indicator of lensing. There exist some unrelated pairs.

4 SUMMARY AND DISCUSSION OF OBSERVATIONS

The entire JVAS and CLASS data set of ~15 000 sources was searched for cases of gravitational lensing on scales of 6 arcsec $\leq \Delta\theta \leq$ 15 arcsec. Only one candidate, J0122+427, remains after follow-up observations with the VLA and MERLIN. However, J0122+427 has a 5-GHz flux density of only 21 mJy, and so it is *not* part of the *statistically complete* JVAS/CLASS sample (see Section 1). Furthermore, recent observations with the WHT do not support the lensing hypothesis; optical emission is detected from position of both radio components but the optical component flux density ratio is about an order of magnitude different from that seen in the radio. In addition, possible structure within the weaker component suggests that the surface brightneses are different.

A sample of lens candidates selected by Hawkins (1997) suggested that the majority of lens systems with image separations between 2 and 8 arcsec have 'dark' galaxies acting as the lensing mass. Jackson et al. (1998) argued against this citing the then 12 JVAS and CLASS lens systems resulting from a search for image separations <6 arcsec. In this sample of 12 systems, all lensing galaxies were detected at optical and/or infrared wavelengths. However, Hawkins (1997) considered several systems with separations >6 arcsec, leading to the possibility that only massive galaxies have very high mass-to-light ratios. The result of the present work with *no* lensing events in the ~10 000 complete sample found within this 'wide' separation range suggests that such massive galaxies, either luminous or dark, are rare.

Of the ~10 000 known optical quasars, at least 9 ambiguous pairs exist with similar redshifts (Kochanek, Falco & Muñoz 1999). If these are examples of gravitational lensing one would expect a similar number of such pairs within a similarly sized radio sample, such as JVAS/CLASS, because gravitational lensing is achromatic. However, we find no lensing events on such scales, strongly supporting the argument of Kochanek et al. (1999) that the ambiguous optical pairs are in fact binary quasars.

5 CONSTRAINTS ON THE CORE RADII OF GALAXY GROUPS AND CLUSTERS

The following section describes a basic Press–Schechter calculation of the number of lensing events expected within the statistically complete JVAS/CLASS sample of 9284 flat-spectrum radio sources with $S_{8.4} \geq 20$ mJy. The singular isothermal sphere and cored isothermal sphere are used as lens models for a range of values of the cosmic density $\Omega_{\rm M}$ and the cosmological constant Ω_Λ (where $\Omega_{\rm M} + \Omega_\Lambda = 1 - \Omega_k$). Throughout, the values $D_{\rm s}$, $D_{\rm d}$, and $D_{\rm ds}$ are the source, lens, and lens-to-source angular diameter distances, using the filled beam approximation.

5.1 Gravitational lensing statistics

The probability that a background source at redshift $z_{\rm s}$ is seen by an observer to be lensed by an intervening massive object at redshift z with velocity dispersion σ_v is given by

$$\tau(z_{\rm s}) = \int_0^{z_{\rm s}} \int_{\sigma_v^{\rm min}}^{\sigma_v^{\rm max}} n(\sigma_v, z)(1+z)^3 \left| c\frac{{\rm d}t}{{\rm d}z} \right| \tilde{\sigma}(\sigma_v, z)\, {\rm d}\sigma_v\, {\rm d}z$$

where $n(\sigma_v,z)$ is the comoving number density of potential lenses at redshift z, $\tilde{\sigma}(\sigma_v,z)$ is the lensing cross-section, and $|c\frac{{\rm d}t}{{\rm d}z}|$ is the line element. To calculate the range of σ_v to integrate over for a given range of image separations ($\Delta\theta$), the following expression is used (cf. Kochanek 1995):

$$\sigma_v = c\left(\frac{\Delta\theta D_{\rm s}}{\Delta x 4\pi D_{\rm ds}}\right)^{\frac{1}{2}}$$

where Δx is the dimensionless image separation. This value is equal to 2 for the singular isothermal sphere lens model, and is calculated numerically for the cored isothermal sphere model.

Following the approach of Kochanek (1995), the Press & Schechter (1974) model is used to estimate the number density of potential lensing masses as a function of redshift and velocity dispersion. The comoving number density of potential lenses at redshift z and velocity dispersion (σ_v, σ_v + dσ_v) can be written

$$n(\sigma_v, z)\, {\rm d}\sigma_v = \frac{3}{(2\pi)^{3/2}} \frac{\delta_{\rm c}(z)}{r_0^3 \sigma_v \sigma} \frac{{\rm d}\ln\sigma}{{\rm d}\ln r_0} \exp\left[-\frac{\delta_{\rm c}^2(z)}{2\sigma^2}\right] {\rm d}\sigma_v.$$

where $\delta_{\rm c}(z)$ is the linear overdensity of a perturbation that has collapsed and virialized at redshift z, σ is the variance of the fluctuation power spectrum, and r_0 is the radius of a halo just before collapse defined by

$$r_0 = \frac{2\sigma_v}{\Delta_{\rm c}^{1/6} \Omega_M^{1/3} H_0 E(z)^{1/3}}$$

where $\Delta_{\rm c}$ is the density contrast and $E(z) = H(z)/H_0$. Expressions for $\delta_{\rm c}(z)$ and $\Delta_{\rm c}$ can be found in Mo, Mao & White (1998) and Bryan & Norman (1998). An expression for the power spectrum $P(k) \propto kT^2(k)$ is taken from Bardeen et al. (1986),

$$T(k) = \frac{\ln(1+2.34q)}{2.34q} \times [1 + 3.89q + (16.1q)^2 + (5.46q)^3 + (6.71q)^4]^{1/4},$$

where $q = k/(h\Gamma)$ Mpc and Γ is the shape parameter given by Sugiyama (1995):

$$\Gamma = \Omega_{\rm M} h \exp(-\Omega_{\rm b} - \Omega_{\rm b}/\Omega_{\rm M}).$$

The normalization of the power spectrum is fixed by perturbations on a scale of $r = 8\,h^{-1}$ Mpc, denoted σ_8, from the expression derived by Viana & Liddle (1996).

Because gravitational lensing amplifies the flux density of background sources, multiply imaged sources will be preferentially

included within a flux density limited sample, an effect referred to as the amplification bias. This is generally a non-trivial effect because source counts increase with decreasing flux density. Following Fukugita & Turner (1991), the bias factor is given by

$$B(S) = \frac{N_{\rm L}(S)}{\tau N(S)}$$

where S is the flux density, $N(S)$ are the number counts of unlensed sources in a sample, τ is the optical depth, and

$$N_{\rm L}(S) = \tau \int_{A'_{\rm min}}^{\infty} A^{-1} N(S/A) P(A)\,{\rm d}A$$

are the number counts of lensed sources. $A'_{\rm min}$ is the minimum total amplification for a multiple imaging event with a maximum flux density ratio limit, the value of which was calculated numerically for the cored isothermal sphere lens model (Section 5.2). Maoz & Rix (1993) state that for a background point source, circular lenses follow the relation

$$P(A)\,{\rm d}A = 2A_{\rm min}^2 A^{-3}\,{\rm d}A, \quad A > A_{\rm min},$$

where $A_{\rm min}$ is the minimum total amplification necessary for a multiple imaging event. The slope of the differential source counts for the statistically complete JVAS/CLASS sample at 5 GHz was derived to be $\beta = 2.09$ where $N(S)\,{\rm d}S \propto S^{-\beta}\,{\rm d}S$.

In order to calculate the cross-section $\tilde{\sigma}$, the mass density profile of the lensing masses must be investigated. The following subsection introduces two such profiles, the singular isothermal sphere and the cored isothermal sphere.

5.2 Isothermal sphere lens models

The singular isothermal sphere density distribution is the simplest reasonable description of a lensing mass from the scale of a single galaxy to the scale of clusters of galaxies. The density profile takes the form (for example Hinshaw & Krauss 1987)

$$\rho(r) = \frac{\sigma_v^2}{2\pi G r^2}.$$

It is convenient to define dimensionless units x and y for the source position in the lens and source planes respectively. Here we define $x = \xi/\xi_0$ where ξ is the actual source position in the lens plane and

$$\xi_0 = 4\pi\left(\frac{\sigma_v}{\rm c}\right)^2 \frac{D_{\rm d} D_{\rm ds}}{D_{\rm s}}.$$

The source position in the source plane is then simply $y = \eta D_{\rm d}/\xi_0 D_{\rm s}$ where η is the actual source position in the source plane.

The cross-section in the lens plane can be derived as

$$\tilde{\sigma} = 16\pi^3\left(\frac{\sigma_v}{\rm c}\right)^4 \left(\frac{D_{\rm d} D_{\rm ds}}{D_{\rm s}}\right)^2 y_R^2. \quad (1)$$

where y_R is the maximum source position to observe a particular image flux density ratio R. For the singular isothermal sphere model it can be shown that

$$y_R = \left(\frac{R-1}{R+1}\right)^2.$$

The cored isothermal sphere density distribution is a modification of the singular isothermal sphere density distribution which removes the central singularity by introduction of a 'core radius'. The density profile takes the form (for example Hinshaw & Krauss 1987)

$$\rho(r) = \frac{\sigma_v^2}{2\pi G(r^2 + r_{\rm c}^2)}.$$

The dimensionless core radius is defined as $x_{\rm c} \equiv r_{\rm c}/\xi_0$. It can be shown that multiple imaging is possible only when $x_{\rm c} < 1/2$. Equation (1) is also applicable to the cored isothermal sphere lens model and the value of y_R was calculated numerically for the limiting flux density ratio of the JVAS/CLASS survey.

5.3 Results

As a preliminary test of the Press–Schechter analysis performed here, a comparison was made with the results of Kochanek (1995), where values of $\Omega_{\rm M} = 1$, $\Omega_\Lambda = 0$, $\Gamma = h = 0.5$, and $\sigma_8 = 1.05$ were used. The optical depth was calculated for multiple imaging with image separations > 5 arcsec and flux density ratios $< 4:1$ for source redshifts of 1, 2 and 3 and was found to agree with the result of Kochanek (1995) to within $\sim$5 per cent in each case.

The results of the Press–Schechter analysis for the JVAS and CLASS 6- to 15-arcsec lens search are shown in Tables 5 and 6. For all models a value of $h = 0.7$ was assumed. The results are based upon a background source sample of 9261 sources, with a redshift distribution identical to that of the Caltech–Jodrell Bank flat-spectrum (CJF) sample (Taylor et al. 1996), which has a mean redshift $\sim$1.3 (Vermeulen et al., unpublished). Whilst this is not an ideal assumption, the redshift distribution of flat-spectrum radio sources does not appear to be significantly changing from that of CJF at lower flux densities (Marlow et al. 2000).

The number of 6- to 15-arcsec lensed objects expected within JVAS and CLASS as a function of $\Omega_{\rm M}$ for $\Omega_\Lambda = 0$ and $\Omega_k = 0$ models using singular isothermal sphere lenses is given in Table 5. Note that the one remaining weak candidate, J0122+427, is *not* contained within the *statistically complete* sample of 9261 sources and so the Poisson likelihood of finding *no* lenses is calculated. For an $\Omega_\Lambda = 0$ universe, $\Omega_{\rm M} < 0.25$ at 3σ. This value agrees with those obtained by a variety of other methods (for a recent review see Primack 2000), but the location of the first acoustic peak in the cosmic microwave background (CMB) anisotropy data strongly suggests that $\Omega_{\rm M} + \Omega_\Lambda = 1$. The currently most favoured pair of

Table 5. The number of lensing events expected in the statistically complete JVAS/CLASS samples using the singular isothermal sphere lens mass model. Column 2 shows the results where $\Omega_\Lambda = 0$, whilst column 3 shows the results where $\Omega_k = 0$.

$\Omega_{\rm M}$	$N\,(\Omega_\Lambda = 0)$	$N\,(\Omega_k = 0)$
0.1	4.06	12.23
0.2	5.76	12.34
0.3	6.37	10.61
0.4	6.80	9.48
0.5	7.51	9.31
0.6	8.16	9.39
0.7	8.80	9.66
0.8	9.50	10.09
0.9	10.31	10.64
1.0	11.30	11.30

Table 6. The number of lensing events, N_{Ω_M}, expected in the statistically complete JVAS/CLASS samples using the cored isothermal sphere lens mass model. A range of values of Ω_M have been used for $\Omega_k = 0$ models. It is clear that the number of lensing events expected is dramatically reduced for high values of the core radius x_c.

x_c	$N_{0.1}$	$N_{0.2}$	$N_{0.3}$	$N_{0.4}$	$N_{0.5}$	$N_{0.6}$	$N_{0.7}$	$N_{0.8}$	$N_{0.9}$	$N_{1.0}$
0.05	13.64	13.49	11.45	10.12	9.85	9.86	10.10	10.52	11.07	11.74
0.10	10.54	10.22	8.57	7.49	7.23	7.19	7.33	7.61	7.99	8.46
0.15	8.26	7.84	6.48	5.60	5.35	5.28	5.36	5.54	5.81	6.14
0.20	6.47	6.00	4.88	4.16	3.92	3.84	3.87	3.99	4.17	4.40
0.25	4.94	4.45	3.56	2.98	2.77	2.68	2.68	2.75	2.86	3.01
0.30	3.68	3.20	2.49	2.05	1.87	1.78	1.76	1.79	1.86	1.95
0.35	2.53	2.09	1.59	1.26	1.12	1.05	1.02	1.03	1.06	1.10
0.40	1.59	1.23	0.89	0.68	0.57	0.52	0.50	0.49	0.50	0.51
0.45	0.17	0.11	0.08	0.05	0.04	0.03	0.03	0.03	0.03	0.03

values of $(\Omega_M, \Omega_\Lambda) = (0.3, 0.7)$ is inconsistent with the lack of observed wide-separation lens systems at 4.2σ *based on a singular isothermal sphere lens mass model*.

The singular nature of the singular isothermal sphere profile is however not physical and in fact increases the probability of lensing compared with more physically realistic models owing to the high surface mass density towards the centre of the mass distribution. Several authors (for example Flores & Primack 1996) have noted that the lensing probability decreases significantly when a core radius is introduced, which removes the central singularity. While there are several such mass profiles discussed in terms of lensing (for example the 'King profile': King 1962; the 'Universal Profile':Navarro, Frenk & White 1997), for simplicity the cored isothermal sphere is used to illustrate the influence of the mass profile in determining the lensing rate within a sample. The effects of using a wider range of mass profiles in the calculation is explained in Keeton & Madau (2001). Table 6 shows the number of lensing events expected within JVAS/CLASS as a function of Ω_M and x_c for the CMB-favoured $\Omega_k = 0$ set of universes. It can be seen immediately that the predicted number of lensing events falls by over an order of magnitude between $x_c = 0$ and $x_c = 0.4$ (obviously the rate falls to 0 as $x_c \rightarrow 0.5$ where multiple imaging can no longer occur). It is clear that it is more useful to place constraints on the value of x_c rather than on the ranges of Ω_M and Ω_Λ, owing to the lower number of lensing events when x_c is large. For the case of no lenses in JVAS and CLASS between 6 and 15 arcsec with $(\Omega_M, \Omega_\Lambda) = (0.3, 0.7)$, the lower limit on the value of x_c is 0.17, 0.27 and 0.38 at 3σ, 2σ and 1σ respectively.

Of course it should be noted that a single value of x_c corresponds to a redshift-dependent range of values of r_c for a given σ_v. However, the majority of lensing masses will occur within a smaller redshift range (typically $0.2 < z_l < 0.5$ for $z_s \sim 1$) than that from the observer to the source, and so the constraints on x_c are still of interest.

6 DISCUSSION

The result of Section 5.3 illustrates the importance of understanding the mass profile of clusters when calculating the number of strong lensing events expected within a survey. Giant arcs produced by cluster lenses, along with X-ray-emitting gas observations, have been used by several authors to place constraints on the parameters which describe the mass profile of clusters (for example Tyson, Wenk & Valdes 1990; Miralda-Escudé 1993; Wu & Hammer 1993). Typically the value of the core radius derived from X-ray cluster gas was several times larger than that from lensing. Bartelmann & Weiss (1994) performed an *N*-body simulation of the mass distribution and X-ray emissivity of a cluster with the aim of resolving the discrepancy between the core radii obtained by each method. They reached the conclusion that the intracluster gas may have been expelled from the cluster galaxies *after* the potential well of the cluster had formed. This is supported by the fact that the observed iron abundance is about one third of the solar abundance, implying a degree of processing of the gas by stars. This would result in the X-ray emission having a smoother distribution than the mass. Although only one cluster was simulated, it was found to have a rather extended core radius $x_c \sim 2$, but also a steeper-than-isothermal surface density profile allowing the occurrence of strong lensing.

In a follow-up paper, Bartelmann, Steinmetz & Weiss (1995) showed that a numerically constructed inhomogeneous mass model could produce more giant arcs than a cored isothermal sphere lens model with the same values of σ_v and r_c by two orders of magnitude. In fact, the simulations showed that the numerical models were of similar efficiency to the singular isothermal sphere model in the production of giant arcs. A comparison of arc statistics within the arcs survey of Le Fevre et al. (1994) was conducted by Hattori, Watanabe & Yamashita (1997) for spherical lens mass models, and even mass distributions with small core radii could not reproduce the large number of giant arcs seen. While Bartelmann et al. (1995) showed that their numerically simulated model produced a similar number of arcs to the singular isothermal sphere model, a lack of resolution within the central region of their simulated cluster could account for this remaining deficiency.

Values of the core radius of lensing clusters have more recently been derived by considering the effect of galaxies within the cluster. An estimate of r_c for Cl0024+1654 was made by Wallington, Kochanek & Koo (1995). They used an elliptical mass profile to model the cluster, and two spherical profiles to model the two galaxies observed near the giant arc structure of the system. The resulting values for the cluster mass profile were $\sigma_v = 1100$–$1400\,\mathrm{km\,s^{-1}}$, with $r_c = (30\text{–}60)\,h^{-1}\,\mathrm{kpc}$, equivalent to $x_c = (0.44\text{–}0.54)\,h^{-1}$. Fischer et al. (1997) considered the case of B0957+561, the first gravitational lens system discovered, where the source is being lensed by a massive galaxy and a cluster of which the galaxy is part. The weakly lensed images of background sources were used to determine the mass profile of the cluster, centred 22 arcsec from the main lens galaxy. Values of $\sigma_v \sim 725\,\mathrm{km\,s^{-1}}$ and $r_c \sim 17\,h^{-1}\,\mathrm{kpc}$ were derived, equivalent to $x_c \sim 0.55\,h^{-1}$. This value of the core radius would make the cluster on its own sub-critical and suggests that the central massive galaxy alone is creating the multiple imaging effect. The additional

mass from the cluster would have the effect of increasing the separation of the lensed images.

Modelling a cluster mass profile with a single sphere or ellipsoid generally does not produce satisfactory results in terms of strong gravitational lensing (for example Cl0024 + 1654 and B0957+561 above). Clusters contain significant high surface mass density substructures in the form of galaxies, which modify the caustic structure of the cluster. Williams, Navarro & Bartelmann (1999) performed *N*-body simulations of cluster formation with CDM in order to examine the core structure and compare these results with those derived from gravitational lensing. They find that for average clusters ($\sigma_v \sim 1000\,\mathrm{km\,s^{-1}}$) the central surface mass density must be enhanced by a massive ($\sim 3 \times 10^{12}\,h^{-1}\,\mathrm{M_\odot}$) galaxy and significant substructure within the cluster to produce the observed rate of strong lensing. This recent result supports the conclusions drawn from the previous work on individual lensing clusters summarized here i.e. the core radius of the surface mass density in clusters of galaxies *on its own* is generally too large to produce multiple images of background sources.

The results presented in this paper suggest that 'wide separation' strong lensing of compact sources is a relatively rare event because the surface mass density of clusters of galaxies (with $400 \lesssim \sigma_v \lesssim 650\,\mathrm{km\,s^{-1}}$) is close to or below critical, as implied by the limits of x_c derived (see above). The results of Bartelmann & Weiss (1994) and Bartelmann et al. (1995) suggest that cluster mass profiles are not well described by isothermal mass profiles, and that substructure within clusters may enhance the probability of finding giant arcs by two orders of magnitude, similar to that of an singular isothermal sphere lens. Of course the main reason that optical arcs are often seen behind clusters, whilst wide separation lensed radio sources are *not*, is that the surface number density of optical galaxies is several orders of magnitude higher at practical detection limits in comparison with radio sources. In addition, these predictions considered extended background sources which can lie across several of the cluster's caustics, creating complex multiple arc images. The JVAS and CLASS search for lensing considers *unresolved* sources which may decrease the number of lensed images seen.

Caution must be exercised when trying to compare the high number of arcs found behind X-ray clusters, which result in a low value of x_c (for example Grossman & Saha 1994; Hattori et al. 1997), and the number of lensing events found from *this* work and the relatively *high* value of x_c thus derived. At least two important selection effects must be noted regarding the X-ray clusters: the most luminous X-ray clusters are selected, typically with very high velocity dispersions; and X-ray luminosity varies as the square of the mass density, and so concentrated clusters with smaller core radii will be preferentially selected.

7 SUMMARY

The JVAS and CLASS wide-separation lens search currently contains only one rather weak candidate for multiple imaging, and this candidate does *not* meet the selection criteria for the *statistically complete* JVAS/CLASS sample. There is *at most* one case of gravitational lensing on these scales from a sample of ~15 000 flat-spectrum radio sources. This strongly supports the argument of Kochanek et al. (1999) that the majority of 3- to 10-arcsec quasar pairs are binary quasars and leads to the conclusion that a population of 'dark' galaxies makes at most a small contribution to the galaxy mass of the 'local' ($z < 1$) universe.

The Press–Schechter mass function was used to predict the number of lensing events expected in JVAS and CLASS with image separations between 6 and 15 arcsec. It is clear that this approach does not yield meaningful constraints on the cosmological parameters because a statistically accurate model of the mass distribution in groups and clusters of galaxies has not been established. However it has been demonstrated that the singular isothermal sphere model predicts approximately an order of magnitude too many lens systems for the range of parameters examined. The addition of a core radius to the isothermal mass model suggests that the parameter should typically be close to the critical radius for multiple imaging.

It is suggested through modelling of known lens systems (for example Wallington et al. 1995; Fischer et al. 1997) and some of the most recent *N*-body simulations (Williams et al. 1999) that it is a massive galaxy which produces the image splitting and the role of the cluster is to increase the image separation. If this is the case, the number of multiple imaging events seen between 6 and 15 arcsec will be significantly affected by the probability of finding a massive galaxy in an appropriate location within a cluster.

ACKNOWLEDGMENTS

The VLA is the Very Large Array and is operated by the National Radio Astronomy Observatory which is a facility of the National Science Foundation operated under cooperative agreement by Associated Universities, Inc. MERLIN is the Multi-Element Radio Linked Interferometer Network and is a national facility operated by the University of Manchester on behalf of PPARC. The WHT is operated on the island of La Palma by the Isaac Newton Group in the Spanish Observatorio del Roque de los Muchachos of the Instituto de Astrofisica de Canarias. This research was supported in part by the European Commission, TMR Programme, Research Network Contract ERBFMRXCT96-0034 'CERES'. PMP also thanks PPARC for the support of a studentship award.

REFERENCES

Bardeen J. M., Bond J. R., Kaiser N., Szalay A. S., 1986, ApJ, 304, 15
Bartelmann M., Weiss A., 1994, A&A, 287, 1
Bartelmann M., Steinmetz M., Weiss A., 1995, A&A, 297, 1
Browne I. W. A., Patnaik A. R., Wilkinson P. N., Wrobel J. M., 1998, MNRAS, 293, 257
Bryan G. L., Norman M. L., 1998, ApJ, 495, 80
Cen R., Gott J. R. I., Ostriker J. P., Turner E. L., 1994, ApJ, 423, 1
Condon J. J., Broderick J. J., Stielstad G. A., 1989, AJ, 97, 1064
Condon J. J., Dickey J. M., Salpeter E. E., 1990, AJ, 99, 1071
Condon J. J., Cotton W. D., Greisen E. W., Yin Q. F., Perley R. A., Taylor G. B., Broderick J. J., 1998, AJ, 115, 1693
Cooray A. R., Grego L., Holzapfel W. L., Joy M., Carlstrom J. E., 1998, AJ, 115, 1388
Feretti L., Giovannini G., 1996, in Ekers R. D., Fanti C., Padrielli L., eds, Proc. IAU. Symp. 175, Extragalactic Radio Sources. Kluwer, Dordrecht, p. 333
Fischer P., Bernstein G., Rhee G., Tyson J. A., 1997, AJ, 113, 521
Flores R. A., Primack J. R., 1996, ApJ, 457, L5
Fukugita M., Turner E. L., 1991, MNRAS, 253, 99
Giovannini G., Tordi M., Feretti L., 1999, New Astron., 4, 141
Grossman S. A., Saha P., 1994, ApJ, 431, 74
Hattori M., Watanabe K., Yamashita K., 1997, A&A, 319, 764
Hawkins M. R. S., 1997, A&A, 328, L25
Hinshaw G., Krauss L. M., 1987, ApJ, 320, 468

Irwin M., Maddox S., McMahon R., 1994, Spectrum, 2, 14
Jackson N., Helbig P., Browne I., Fassnacht C. D., Koopmans L., Marlow D., Wilkinson P. N., 1998, A&A, 334, L33
Keeton C. R., Madau P., 2001, ApJ, 549, L25
King I., 1962, AJ, 67, 471
Kochanek C. S., 1995, ApJ, 453, 545
Kochanek C. S., Falco E. E., Muñoz J. A., 1999, ApJ, 510, 590
Le Fevre O., Hammer F., Angonin M. C., Gioia I. M., Luppino G. A., 1994, ApJ, 422, L5
Lehar J., Buchalter A., McMahon R. G., Kochanek C. S., Muxlow T. W. B., 2001, ApJ, 547, 60
Marlow D. R., Rusin D., Jackson N., Wilkinson P. N., Browne I. W. A., Koopmans L., 2000, AJ, 119, 2629
Miralda-Escudé J., 1993, ApJ, 403, 497
Maoz D., Rix H., 1993, ApJ, 416, 425
Mo H. J., Mao S., White S. D. M., 1998, MNRAS, 295, 319
Myers S. T. et al., 1995, ApJ, 447, L5
Navarro J. F., Frenk C. S., White S. D. M., 1997, ApJ, 490, 493
Patnaik A. R., Browne I. W. A., Wilkinson P. N., Wrobel J. M., 1992, MNRAS, 254, 655
Pearson T. J., Shepherd M. C., Taylor G. B., Myers S. T., 1994, Am. Astron. Soc. Meeting Vol. 185, p. 0808
Press W. H., Schechter P., 1974, ApJ, 187, 425
Primack J. R., 2000, preprint (astro-ph/0007187)
Refsdal S., 1964, MNRAS, 128, 307
Shepherd M. C., 1997, in Hunt G., Payne H. E., eds, ASP Conf. Ser. Vol. 125, Astronomical Data Analysis Software and Systems V. Astron. Soc. Pac., San Francisco, p. 77
Sugiyama N., 1995, ApJS, 100, 281
Taylor G. B., Vermeulen R. C., Readhead A. C. S., Pearson T. J., Henstock D. R., Wilkinson P. N., 1996, ApJS, 107, 37
Tyson J. A., Wenk R. A., Valdes F., 1990, ApJ, 349, L1
Viana P. T. P., Liddle A. R., 1996, MNRAS, 281, 323
Wallington S., Kochanek C. S., Koo D. C., 1995, ApJ, 441, 58
Wambsganss J., Cen R., Ostriker J. P., Turner E. L., 1995, Sci, 268, 274
Wilkinson P. N., Browne I. W. A., Patnaik A. R., Wrobel J. M., 1998, MNRAS, 300, 790
Williams L. L. R., Navarro J. F., Bartelmann M., 1999, ApJ, 527, 535
Wu X., Hammer F., 1993, MNRAS, 262, 187
Zhao J., Burns J. O., Owen F. N., 1989, AJ, 98, 64

This paper has been typeset from a TEX/LATEX file prepared by the author.